Response spectral model for forward-directivity ground motion in the near-fault area

R. Rupakhety, S. U. Sigurðsson & R. Sigbjörnsson
Earthquake Engineering Research Centre (EERC), University of Iceland

15 WCEE
LISBOA 2012

SUMMARY:
We present a new model that can be used to construct the response spectra of near-fault ground motions having pulse-like waveforms. The model is calibrated by using a large set of recorded accelerograms. The shape of the pseudo-velocity spectrum (*PSV*) is modelled as a continuous function of the single-degree-of-freedom (SDOF) natural period. Magnitude dependence of spectral shapes is built into the model, which also includes parameters accounting for effects of viscous damping. An empirical equation for peak ground velocity (*PGV*) is provided to scale the pseudo-velocity spectral shapes, obtaining the absolute *PSV*, which is easily converted to the more commonly used pseudo-acceleration spectrum (*PSA*). A framework for quantifying the uncertainties in the *PGV*, as well as the spectral shapes, is presented in the form of simple equations. Finally, equations to estimate force reduction factors of elastoplastic systems for several levels of target displacement ductilities are also presented.

Keywords: near-fault ground motion, response spectra, peak ground velocity, force reduction factor

1. INTRODUCTION

Near-fault ground motions are known to be a potential cause of severe damage to engineering structures. They usually carry a strong long-period pulse in their velocity records. Directivity effects (see Somerville et al., 1997) and permanent displacement effects (see Abrahamson, 2000) have been identified as the most common features of near-fault ground motions. This study is focused on forward-directivity effects in the near-fault region and characterization of elastic as well as inelastic response spectra of elastic-perfectly-plastic single-degree-of-freedom (SDOF) systems.

The most important features of these ground motions are considered as the amplitude and frequency of the dominant velocity pulse contained in their time series. The amplitude of the pulse is representative of the peak ground velocity. If the pulse were a simple harmonic with infinite duration, the *PSV* would exhibit a peak at a SDOF period exactly equal to the pulse period. However, near-fault velocity pulses are of finite duration, and the period at which *PSV* is the maximum is not exactly equal to the pulse period, but yet, in most cases, very close to it. In this work we quantify the amplitude of ground motion by the PGV, and its frequency content is characterized by a predominant period, which is, in this work, defined as the period where 5% damped linear-elastic *PSV* reaches its peak value. If more than one peaks of comparable amplitude exist, then the longest period is considered.

We present robust empirical equations to estimate *PGV* and predominant period from earthquake size, source-to-site distance, and other relevant parameters. We then present analytical equations of *PGV*-normalized *PSV* (termed here as spectral shapes) as a continuous function of the SDOF natural period and its level of viscous damping. Finally, characteristics of inelastic response are studied, and equations relating strength reduction factors to displacement ductility of elasto-plastic SDOF systems are presented. The models presented here are calibrated by using 93 accelerograms obtained from 29 worldwide earthquakes. More information on the data can be found in Rupakhety et al. (2011).

2. RELATIONSHIP BETWEEN PREDOMINANT PERIOD AND SEISMIC MOMENT

Predominant period of ground motion, denoted T_d is found to scale linearly with seismic moment, and its corresponding relationship between moment magnitude (M_w) and can hence be modeled by the following expression

$$\log\left(T_d\right) = \alpha M_w + \beta + \varepsilon \tag{2.1}$$

where α and β are model coefficients determined by regression analysis and ε is residual error treated as a Gaussian-distributed random variable with zero mean and standard deviation σ. The model of Eqn. 2.1 was calibrated by using least squares regression. Further details regarding the data used in regression can be found in Rupakhety et al. (2011). The regression parameters were found to be $\alpha = 0.47$, $\beta = -2.87$, and $\sigma = 0.18$. The regression line and data points are presented in Fig. 1. The mean value predicted by regression is shown with the solid line, while dashed lines correspond to $\text{mean} \pm 2\sigma$ levels. The distribution of ε is compared with a standard normal distribution in the small inset in the top-left corner of Fig. 1.

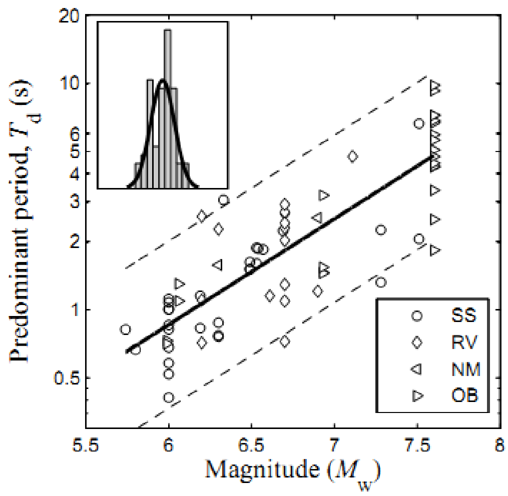

Figure 1. Scaling of T_d with M_w. The Solid line is the mean value of a least squares line fitted to the data, while the dashed lines correspond to mean $\pm 2\sigma$. Different markers are used for strike-slip (SS), reverse (RV), normal (NM), and oblique (OB) faulting mechanisms as indicated in the legend.

3. ATTENUATION EQUATION FOR *PGV*

The functional form adopted for the attenuation equation is

$$\log\left(PGV_{ij}\right) = \begin{cases} a + bM_w + cM_w^2 + d\log\left(R^2 + e^2\right) + \eta_i + \varepsilon_{ij} & \text{if } M_w \le M_{sat} \\ a + bM_{sat} + cM_{sat}^2 + d\log\left(R^2 + e^2\right) + \eta_i + \varepsilon_{ij} & \text{otherwise} \end{cases} \tag{3.1}$$

where PGV_{ij} is the PGV (in m/s) of the jth recording from the ith event; M_w is the moment magnitude of event i; R is the distance (measured in km) of the jth recording obtained from the ith event; a, b, c, d, e, and M_{sat} are regression parameters; and η_i and ε_{ij} represent inter- and intraevent variations. The error terms η_i and ε_{ij} are assumed to be independent, normally-distributed random variables with variances σ_1^2 and σ_2^2, respectively. The total standard deviation associated with estimated *PGV* can be computed from the following equation.

$$\sigma_t = \sqrt{\sigma_1^2 + \sigma_2^2} \tag{3.2}$$

For distance measure R, we use Joyner-Boore distance (r_{JB}) when rupture model is available and epicentral distance (r_{epi}) otherwise. Furthermore, we select only those stations within 30 km from the source. More information regarding the data used in regression analysis can be found in Rupakhety et al. (2011). The regression parameters were calibrated by using the maximum likelihood method of Joyner and Boore (1993). Regression constants and associated values of standard deviations are shown in Table 1

Table 1. Regression coefficients for the model of Eqn. 3.1.

a	b	c	d	e	M_{sat}	σ_1	σ_2	σ_t
-5.17	1.98	-0.14	-0.10	0.75	7.0	0.081	0.135	0.16

In Fig. 2 we compare the model of Eqn. 3.1 and the associated parameters of Table 1 with models proposed by Bray and Rodriguez-Marek (2004), Somerville (1998), Alavi and Krawinkler (2000), and Halldórsson et al. (2011), hereafter called as B&R-M04, S98, A&K00, HM&P10, respectively. These authors use the closest distance to rupture as their distance metric. For comparing their model with ours, we assume a vertical strike-slip event. The thick black line in Fig. 2 corresponds to the mean prediction of the proposed model, while upper and lower fractals with 2 standard deviations are shown by black dashed lines. Circles indicate observed values of *PGV*. *PGV* corresponding to all magnitudes are shown, and the model predictions are computed at magnitude 6.6, which is also the mean magnitude of our data. The mean prediction of B&R-M04 is shown with the solid blue line. The dashed red line, the dashed blue line, and the solid red line represent mean predictions of S98, A&K00, and HM&P10, respectively. We note that the magnitude scaling parameters of A&K00 and S98 are high, and our data do not support such a strong magnitude dependence of *PGV*. On the other hand, magnitude scaling is zero in HM&P10. The attenuation of *PGV* above distances greater than 7 km is very fast in the Model of Bray and Rodriguez-Marek. Fast attenuation in HM&P10's model is related to their functional form. In their model, *PGV* attenuates exponentially with distance. Such exponential attenuation is not supported by our data, as shown in Fig. 2.

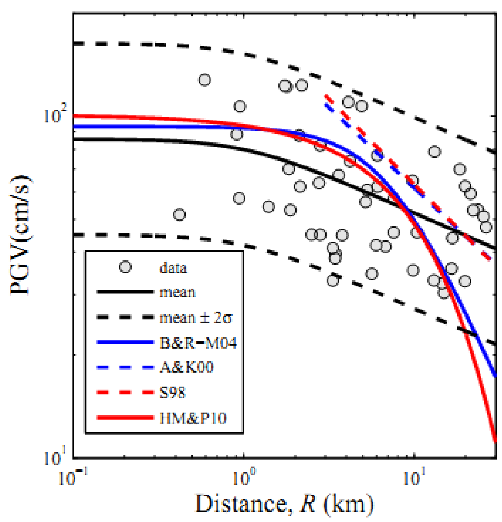

Figure 2. Comparison of the model of Eqn. 3.1 with observed data (circles) and the models of other authors as

indicated in the legend (see text above for legend keys).

4. ELASTIC RESPONSE SPECTRA

Accelerograms from large earthquakes in the recent past have shown that response spectra of near-fault ground motions, mainly of those affected by forward-directivity effects, are different from those of far-fault ones. One of the characteristic differences between the two is the narrow-banded spectral structure of the former. Response spectra of forward-directivity-affected near-fault ground motion exhibit spectral peak values in a narrow band of periods near the predominant period of ground motion. Predominant period increases with increasing earthquake magnitude, and thus the response spectra are strongly influenced by earthquake magnitude. The differences in the response of structures to near-fault and far-fault ground motions imply that design spectra, derived from more far-fault accelerograms than near-fault ones, are biased. They are not capable of capturing the impulsive nature of near-fault ground motion and often lead to unreliable estimates of seismic action on engineering structures located near an earthquake fault. Therefore, it is essential to develop design spectra specifically suitable for ground motion in near-fault area. We propose response spectral model applicable strictly to near-fault ground motion exhibiting forward-directivity effects. The proposed model is based on recorded accelerograms within 30 km from the fault generated by earthquakes ranging in magnitude between 5.5 and 7.6. This model should not be extrapolated in terms of earthquake magnitude or source to site distance. The *PSV* normalized by *PGV* is termed as spectral shape, and represented by the equation

$$PSV_n = \left[I_1 \exp\left\{-0.5\left(\ln\left(T_n\right)+1.4\right)^2\right\} + \left(4.92-0.58M_w\right)\left\{\left(1-\left(\frac{T_n}{T_d}\right)^2\right)^2 + 4D_m^2\left(\frac{T_n}{T_d}\right)^2\right\}^{-0.5}\right] T_n \tag{4.1}$$

where T_n is the undamped natural period of the SDOF system; I_1 and D_m are model parameters that depend on earthquake magnitude and viscous damping ratio of the system and T_d is the average predominant period of ground motion given by Eqn. 2.1. To incorporate the magnitude dependence of spectral shapes, we divided the available ground motion data into several magnitude groups and calibrated the model for each group separately. Further details regarding the calibration process can be found in Rupakhety et al. (2011). The calibrated model parameters are presented in Table 2. The model parameters are expressed as a function of the damping ratio (ζ) expressed as a percentage of the critical damping ratio.

The comparisons of the simulated spectral shapes with those computed from recorded accelerograms are shown in Fig. 3, and Fig. 4, for 2% and 20% damping, respectively. The grey and the dark lines in these figures represent the spectral shapes corresponding to recorded data and the proposed model, respectively. The results indicate that the proposed model accurately simulates the spectral shapes of recorded near-fault accelerograms for a wide range of damping ratios.

Table 2. Parameters of Eqn. 4.1 for different magnitude ranges and damping ratios

Magnitude range	I_1	D_m
$5.5 \le M_w \le 6.0$	$0.320\zeta^{-0.5}$	$1.54\zeta + 0.39$
$6.0 \le M_w \le 6.3$	$0.239\zeta^{-0.5}$	$1.73\zeta + 0.44$
$6.3 \le M_w \le 6.6$	$0.211\zeta^{-0.5}$	$2.41\zeta + 0.47$
$6.6 \le M_w \le 6.8$	$0.204\zeta^{-0.5}$	$2.82\zeta + 0.50$
$6.8 \le M_w \le 7.3$	$0.283\zeta^{-0.5}$	$4.18\zeta + 0.58$
$7.3 \le M_w \le 7.6$	$0.242\zeta^{-0.5}$	$3.38\zeta + 0.59$

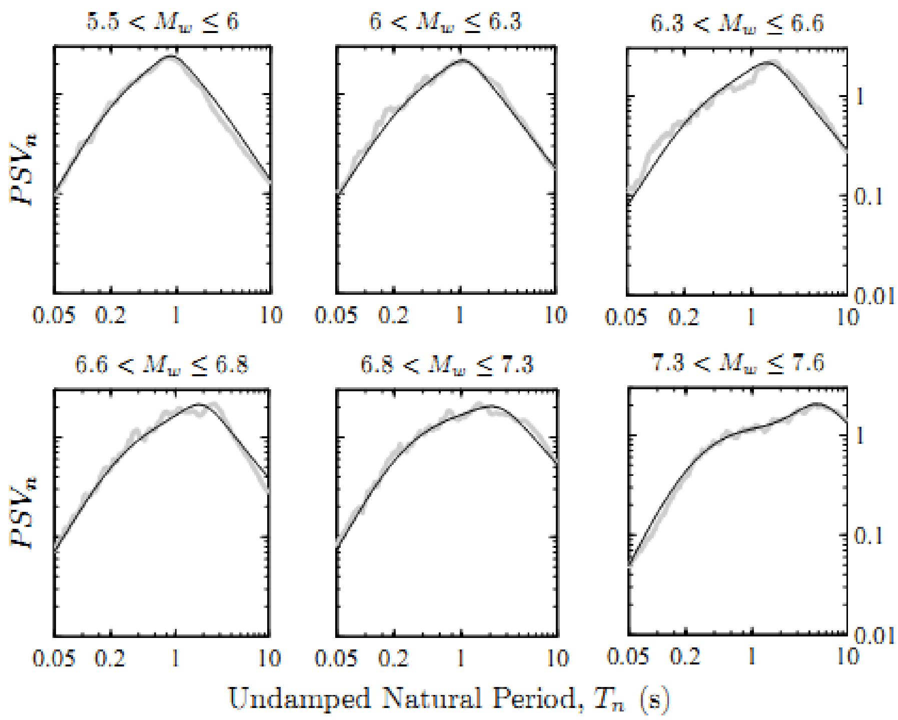

Figure 3. Comparison of 2% damped mean spectral shapes with the ones simulated from Eqn. 4.1 and Table 2.

.

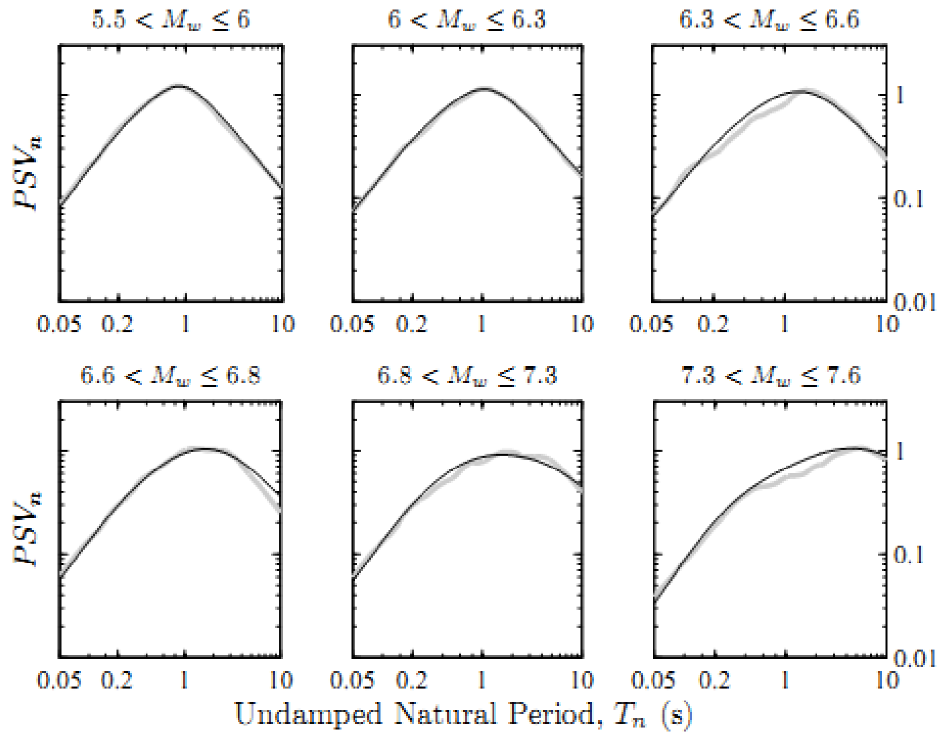

Figure 4. Comparison of 20% damped mean spectral shapes with the ones simulated from Eqn. 4.1 and Table 2.

The standard deviations of spectral shapes in base 10 logarithmic scale are denoted here as $\sigma_{\log PSV_n}$. The variation of these standard deviations with natural period of SDOF system is shown in Fig. 5. Note that the T_n axis is in logarithmic scale. The figure clearly shows that standard deviation reduces as the damping level increases. This is because as damping ratio increases, spectral shapes become smoother. The decrease in the standard deviation of residuals with increasing damping level is the largest in the high-frequency region. We found that uncertainty in spectral shapes predicted by our model is smallest in the range $0.2s < T_n < 4s$ .This is, in most cases, the period range of greatest interest for engineering design. We also notice that the variation of $\sigma_{\log PSV_n}$ with T_n can be approximated by a simple curve as represented by the black line in Fig. 6 for 5% damped systems. The equation related to this approximation is the following.

$$\sigma_{\log PSV_n} = \begin{cases} 0.18 - 0.04\sin\left[2.9\left(\log T_n - 1.7\right)\right] & \text{if } \ -1.73 < \log T_n < 1.0 \\ 0.16 & \text{if } \ \log T_n \le -1.73 \end{cases} \tag{4.2}$$

We suggest this approximation function, which is similar to the computed values of $\sigma_{\log PSV_n}$, to avoid a long list of $\sigma_{\log PSV_n}$ at discrete T_n values. Equation 4.2 corresponds to 5%-damped systems. For higher levels of damping, the standard deviations are smaller. On average it was found that standard deviation for damping ratios of 0.02, 0.07, 0.08, 0.1, 0.12, 0.14, 0.17, and 0.2 were 1.06, 0.98, 0.97, 0.95, 0.93, 0.92, 0.90, and 0.88 times that for 5% damped system, respectively. In order to compute the standard deviation of PSV from $\sigma_{\log PSV_n}$ and $\sigma_{\log PGV}$, the correlation between PSV_n and PGV need to be established. The computed coefficients of these correlation for our data was found to be negative (-0.2 to -0.3) between SDOF periods of 0.01s and 1s beyond which it increased to 0.3 at a SDOF period of 2s, and then decreased steadily to 0 at about 10s. Because these coefficients are small, PSV_n and PGV can be assumed to be uncorrelated, and the uncertainty in PSV can be approximated as

$$\sigma_{\log PSV} = \sqrt{\left(\sigma_{\log PSV_n}\right)^2 + \left(\sigma_{\log PGV}\right)^2}\ .$$

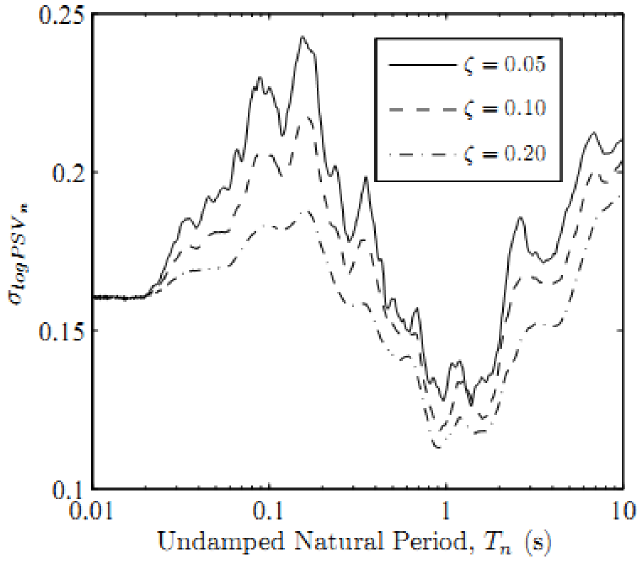

Figure 5. Standard deviation of residuals of spectral shapes for three different levels of viscous damping.

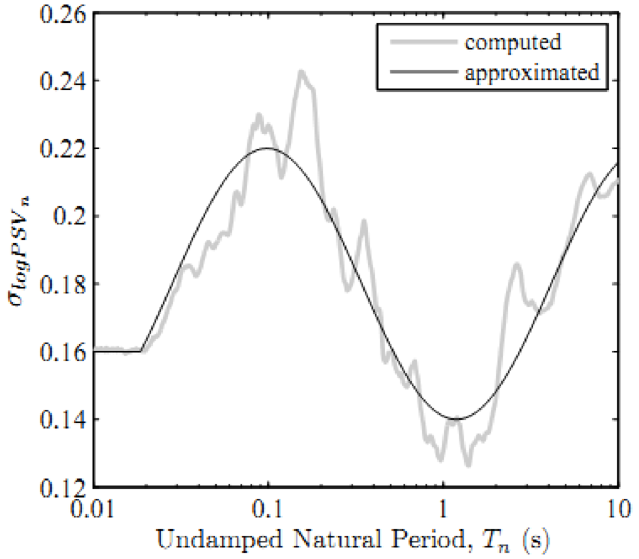

Figure 6. Standard deviation of residuals for 5% damped spectral shapes as a function of T_n.

5. INELASTIC RESPONSE SPECTRA AND FORCE REDUCTION FACTORS

Force-based design of engineering structures for earthquake resistance generally requires inelastic response spectra of SDOF systems to estimate design lateral strengths. Inelastic response spectra for earthquake ground motion are typically constructed by reducing elastic response spectra by the so-called force reduction factor or structural behaviour factor. Hysteretic energy dissipation during inelastic deformation is a major contributor to these reduction factors apart from damping and structural over-strength. The reduction in design forces due to hysteretic energy dissipation $\left(R_\mu\right)$ is defined as the ratio of elastic strength demand to inelastic strength demand required to maintain a displacement ductility (μ) less than or equal to a pre-determined target ductility ratio when subjected to the same excitation. We present relationship between force reduction factor and displacement ductility of elastic-perfectly-plastic system in the form of following equation.

$$R_\mu = [\mu - 1]\psi(T_n) + 1 \tag{5.1}$$

$$\psi(T_n) = \frac{T_n - \gamma}{\gamma \exp(\tau T_n)} + 1 \tag{5.2}$$

In Eqns. 5.1 and 5.2, the constants γ, and τ are functions of μ and were accordingly calibrated using mean reduction factors computed from recorded ground motions. The reduction factors given by these equations satisfy the condition $R_\mu \to 1$ as $T_n \to 0$. As $T_n \to \infty$, the force reduction factor given by our equations approaches μ. The constants of Eqns. 5.1 and 5.2 are presented in Table 3. Fig. 7 compares mean force reduction factors with the proposed equations. Note that the match between the average force reduction factors and the approximate ones given by Eqns. 5.1 and 5.2 shows some differences at long periods. Considering the uncertainty in long-period response spectral ordinates, the calibration of the constants were judged based on structural periods up to about 4s. Even though force reduction factors are presented in Fig. 7 up to structural periods of 10 s, it should be noted that the model is constrained to follow the equal displacement rule at long periods.

Table 3. Parameters of Eqns. 6 and 7 describing the $R_\mu - \mu - T_n$ relationship

μ	γ	τ
1.5	0.50	6.00
2.0	1.00	4.50
3.0	2.00	3.00
4.0	2.50	2.00
5.0	3.00	1.75
6.0	3.25	1.50

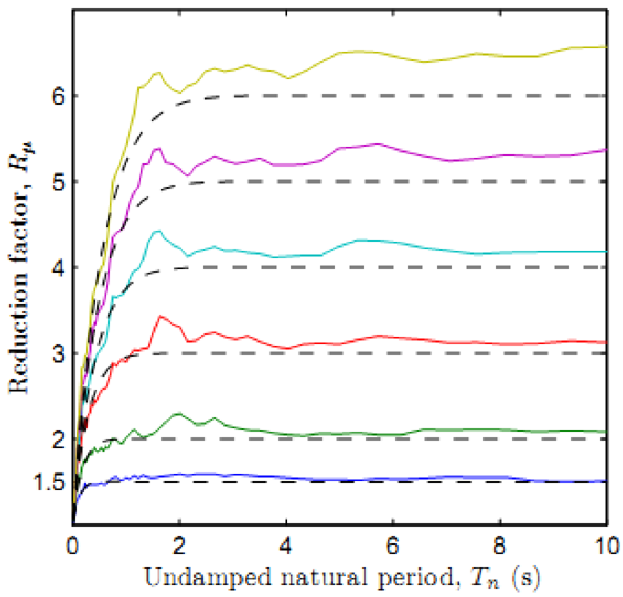

Figure 7. Comparison of mean force reduction factors (solid lines) with the idealized ones (dashed lines) given by Eqns. 5.1 and 5.2 for displacement ductilities of 1.5, 2, 3, 4, 5, and 6.

6. CONCLUSIONS

We present quantitative descriptions of near-fault ground motions in terms of their amplitude and frequency content based on recorded accelerograms. The period where 5% damped pseudo-spectral velocity contains a clear peak is proposed as a measure of predominant period (T_d) of forward-directivity affected near-fault ground motions. The main advantage of this definition is that, unlike pulse period as defined by various authors, this measure is unambiguous and is easily calculated. A robust equation is developed to relate T_d to earthquake magnitude. The relationship between T_d and M_w is similar to scaling relations between pulse period and magnitude proposed by different researchers in the past

The amplitude of near-fault ground motions is quantified in terms of peak ground velocity (*PGV*), and present empirical equations for estimating it as a function of earthquake magnitude and source-to-site distance. However, we found that the available data are not sufficient to constrain a reliable model for the effects of source mechanism and local site conditions. The dependence of *PGV* on moment magnitude is observed to be weak.

Properties of elastic response spectra of forward-directivity-affected near-fault ground motion are discussed in depth. A simple model is proposed to estimate mean spectral shapes of SDOF response to such ground motions. The proposed analytical model is a continuous function of the undamped natural period of SDOF oscillators, and its parameters are magnitude dependent. The model is calibrated by using recorded ground motions. The dependence of the parameters of the proposed model on earthquake size is investigated, constraining their relationship in a step-by-step manner. It was found that several parameters of the model can be effectively expressed in terms of earthquake size, thereby reducing the number of free variables.

In addition, the effects of viscous damping ratio on spectral shapes were thoroughly examined. By studying spectral shapes for different levels of viscous damping, we were able to express the parameters of the spectral shape model as a continuous function of damping ratio. This avoids the use of so-called damping correction factors commonly used to derive response spectra for various levels of damping from that corresponding to 5% of critical damping. The proposed model is found to have small uncertainties in the period range of common engineering structures, whereas uncertainties concerned with very high frequencies are larger. The standard deviation of the residuals of the proposed model was found to be smaller for highly damped systems. The proposed model can be used with any reliable attenuation model of *PGV* to estimate the elastic response spectra for forward-directivity ground motion in the near-fault area. Finally, constant-ductility spectra of elasto-plastic SDOF systems are studied for ductility ratios ranging from 1.5 to 6. An approximate equation to estimate force reduction factors as a function of displacement ductility and SDOF period is proposed.

AKCNOWLEDGEMENT

The financial support provided by the University of Iceland Research Fund and Landsvirkjun´s Energy Research Fund is gratefully acknowledged.

REFERENCES

Abrahamson, N.A. (2000) Effects of rupture directivity on probabilistic seismic hazard analysis. *6th International Conference on Seismic Zonation: Managing Earthquake Risk in the 21st Century*, Earthquake Engineering Research Institute, University of California, Berkeley.

Alavi, B. and Krawinkler, H. (2000) Effects of near-fault ground motions on frame structures. Tech. Rep. 138, John A Blume Earthquake Engineering Center, Stanford University, Stanford, California.

Bray, J.D. and Rodriguez-Marek, A. (2004) Characterization of forward-directivity ground motions in the near-fault region. *Soil Dynamics and Earthquake Engineering* **24:11**, 815–828.

Halldorsson, B., Mavroeidis, G.P. and Papageorgiou A.S. (2010) Near-Fault and Far-Field strong ground motion simulation for earthquake engineering applications using the specific barrier model. *ASCE Journal of Structural Engineering* **137:3**, 433-445.

Joyner, W.B. and Boore, D.M. (1993) Methods for regression analysis of strong-motion data. *Bulletin of the Seismological Society of America* **83:2**, 469–487.

Rupakhety, R., Sigurðsson, S.U., Papageorgiou, A.S. and Sigbjörnsson, R. (2011) Quantification of ground-motion parameters and response spectra in the near-fault region. *Bulletin of Earthquake Engineering*, **9:4**, 893-930.

Somerville, P.G. (1998) Development of an improved representation of near-fault ground motions. SMIP98-CDMG, Oakland, California, 1–20.

Somerville, P.G. (2000) Magnitude scaling of near fault ground motions. *International Workshop on Annual Commemoration of Chi-Chi earthquake*, 18–20.